

Lightning Chemistry on Earth-like Exoplanets

Aleksandra Ardaseva,¹ Paul B. Rimmer,^{1*} Ingo Waldmann,² Marco Rocchetto,²
Sergei N. Yurchenko,² Christiane Helling,¹ Jonathan Tennyson²

¹Centre for Exoplanet Science, SUPA, School of Physics and Astronomy, University of St Andrews, North Haugh, St Andrews, KY16 9SS, UK

²Department of Physics and Astronomy, University College London, London, WC1E 6BT, UK

Accepted XXX. Received YYY; in original form ZZZ

ABSTRACT

We present a model for lightning shock induced chemistry that can be applied to atmospheres of arbitrary H/C/N/O chemistry, hence for extrasolar planets and brown dwarfs. The model couples hydrodynamics and the STAND2015 kinetic gas-phase chemistry. For an exoplanet analogue to the contemporary Earth, our model predicts NO and NO₂ yields in agreement with observation. We predict height-dependent mixing ratios during a storm soon after a lightning shock of NO $\approx 10^{-3}$ at 40 km and NO₂ $\approx 10^{-4}$ below 40 km, with O₃ reduced to trace quantities ($\ll 10^{-10}$). For an Earth-like exoplanet with a CO₂/N₂ dominated atmosphere and with an extremely intense lightning storm over its entire surface, we predict significant changes in the amount of NO, NO₂, O₃, H₂O, H₂, and predict significant abundance of C₂N. We find that, for the Early Earth, O₂ is formed in large quantities by lightning but is rapidly processed by the photochemistry, consistent with previous work on lightning. The effect of persistent global lightning storms are predicted to be significant, primarily due to NO₂, with the largest spectral features present at $\sim 3.4 \mu\text{m}$ and $\sim 6.2 \mu\text{m}$. The features within the transmission spectrum are on the order of 1 ppm and therefore are not likely detectable with JWST. Depending on its spectral properties, C₂N could be a key tracer for lightning on Earth-like exoplanets with a N₂/CO₂ bulk atmosphere, unless destroyed by yet unknown chemical reactions.

Key words: astrobiology – planetary systems: Earth – physical data and processes: hydrodynamics – physical data and processes: molecular processes – astronomical instrumentation, methods, and techniques: atmospheric effects

1 INTRODUCTION

A large number of exoplanets have been discovered over the last few years¹. They differ by the location, characteristics of the host star, and both chemical and physical compositions. Recently, candidate rocky planets within the “liquid water” habitable zone of their star have been discovered: the seven TRAPPIST planets (Gillon et al. 2016; Gillon et al. 2017); and Proxima b (Anglada-Escudé et al. 2016). Transmission spectra of TRAPPIST-1b and TRAPPIST-1c hint at a cloudy atmosphere obscuring spectral signatures (de Wit et al. 2016). The discovery of these planets has further propelled already significant interest into the composition of atmospheres and clouds on potentially habitable exoplanets (e.g Kreidberg & Loeb 2016). Kane et al. (2016) have made the first attempt at compiling a catalogue of poten-

tially habitable exoplanets, using various definitions of the liquid water habitable zone as the identifying criteria.

Clouds, and physical processes related to clouds, are of great interest for determining how probable it would be for life to have arisen on rocky exoplanets, by stabilizing the temperature and effectively expanding the habitable zone (Yang et al. 2013) and by introducing the possibility for lightning discharges, which may generate prebiotic chemistry (Miller 1953). An increasing body of evidence shows that the presence of clouds in exoplanet atmospheres is ubiquitous (e.g. Bean et al. 2010; Sing et al. 2011; Wordsworth et al. 2011; Radigan et al. 2012). These clouds are comprised of particles made of a mix of materials at a rich variety and for which there are often no clear analogues to be found within our solar system.

The structure and composition of the clouds change dependent on the local thermodynamic conditions and the availability, or lack, of nucleating sites such as ocean spray, volcanic ash, and sand. Also the cloud particle size distribution changes over the extent of the atmosphere and over

* E-mail: pr33@st-andrews.ac.uk

¹ <http://exoplanet.eu/>

time. The cloud dynamics, in conjunction with charging processes, can result in significant electric fields spanning large distances. This is because cloud particles carry an excess of positive or negative charge over a great distance, resulting in a large-scale charge separation. The electric field may initiate a discharge, such as lightning, in order to restore that balance (Beasley et al. 1982).

At present, there is only one definitive example of a habitable planet, the Earth, and therefore our present investigation into exoplanetary lightning will focus on Earth analogues. Understanding lightning on these planets, compared to lightning on Earth, is potentially important both for investigating habitability beyond the question of surface liquid water, and for gaining insight into the physical processes on rocky exoplanets, such as exoplanetary global electric circuits (Helling et al. 2016).

Earth-like exoplanets, similarly sized rocky planets with a Sun-like host star, have an occurrence rate of 0.51 planet per star estimated from statistics on the available sample of exoplanets (Dressing et al. 2013). The spectral features of Earth-like exoplanets have already been extensively modelled for a diversity of UV fields by Rugheimer et al. (2013). The varying amount of water on the surface is predicted to have a considerable effect on the rate of lightning. We expect dry, rocky planets to have lightning flash densities equal to $17.0 - 28.9$ flashes $\text{km}^{-2} \text{yr}^{-1}$, whereas Earth-sized planets containing water on their surface would show smaller frequency of only $0.3 - 0.6$ flashes $\text{km}^{-2} \text{yr}^{-1}$ (Hodosán et al. 2016b).

One of the most detailed observational studies of lightning on Earth was carried by Orville (1968a,b,c). Orville performed a time-resolved spectroscopy with the resolution of $5 \mu\text{s}$ on multiple lightning flashes. Using NII emission lines, Orville approximated the peak value of the temperature to lie within the range of $28000 - 31000$ K. This value is obtained from 7 flash spectra and the peak temperature is widely accepted to be $T_{\text{gas}} = 30000$ K. The number density inside the lightning channel is estimated from the $\text{H}\alpha$ broadening, assuming the broadening is caused by the Stark effect only. The spectrum of only one lightning flash showed this feature, therefore it is difficult to determine the uncertainty in the number density; the temperature is better constrained. In Orville's model, the peak pressure is approximated to equal $P_{\text{in}} = 8$ atm, when the pressure of ambient medium is $P_{\text{gas}} = 1$ atm. The pressure is determined experimentally from the experimentally measured equation of state of air at temperatures up to 24000 K (Gilmore 1955).

High temperatures in the lightning channel are very favourable for the dissociation of molecular nitrogen N_2 – a very stable molecule with the dissociation energy being 9.756 eV (Frost & McDowell 1956). The separated nitrogen atoms then participate in neutral Zel'dovich reactions 2 and 1 to form nitric oxide (Zel'dovich & Raizer 2002).



Borucki & Chameides (1984) conclude that approximately 10^{10} kg of both NO and NO_2 is produced in the atmosphere of Earth per year as a consequence of thunderstorms. This makes nitric oxide a signature molecule of lightning on present-day Earth. Price et al. (1997) observed and characterised the chemical impact of lightning on the atmosphere

of the contemporary Earth. This work showed that the effect of lightning on NO and NO_2 is dwarfed by the anthropogenic sources of these molecules.

The ability to dissociate N_2 also provides a potential route for the formation of complex molecules and amino acids, as shown in the Miller-Urey experiment as long as it occurs in favourable chemical environment. Experimentally, the lightning is investigated using laser-induced plasma (LIP) (Jebens et al. 1992; Navarro-González et al. 2001). This approach allows to reach temperatures inside the channel up to $\approx 10^4$ K and has provided insight on how to best link observations of lightning-induced chemistry to theoretical models.

A detailed model of the chemical impact of lightning shocks for atmospheres of a range of compositions will be needed in order to find what effect various flash rates would have on the global chemistry for the diverse set of observed exoplanets. In addition, a coupled hydrodynamic shock model of lightning and chemical shock model will be useful for studies of atmospheric chemistry during lightning storms and of the effect of lightning on chemistry for the Early Earth.

In order to aid in this investigation, we present a lightning model, in which we take existing hydrodynamic and chemical kinetic models of lightning shock induced chemistry, and couple them in order to predict the chemical effects of lightning within atmospheres of arbitrary H/C/N/O chemistry. Our's is the only atmospheric model to account for lightning beyond adding chemical lightning yields as source terms within the atmosphere. Given our focus in this work, this model is here applied specifically for the Contemporary and Early Earth, and makes new predictions for lightning on both the Contemporary and Early Earth. We determine the impact of an intense global lightning storm on the transmission and emission spectrum of Earth-like exoplanets and then discuss the possibility of observing spectral signatures of lightning in this extreme case.

We start by describing the computational model and initial conditions in Section 2. The setup of hydrodynamical shock model and a follow-up comparison with Orville's data is discussed in 2.1. The chemical kinetics network STAND is described in 2.2. We then proceed in 3.1 with an overview and a discussion of the resulting impact of lightning onto the Contemporary Earth atmosphere. The section 3.2 includes the analysis of lightning on Early Earth atmosphere. The hypothetical spectra of Earth-like planets with strong lightning activity is presented in section 4.

2 APPROACH

Here we lay out the methodology for our coupled hydrodynamic chemical kinetics model of the lightning discharge. We use the ATHENA MHD code (Stone et al. 2008) to develop the 2D lightning shock model. ATHENA implements algorithms that allow the use of static and adaptive mesh refinement which solves the conservation of mass, momentum, and energy through the grid (see Appendix A). The code has been extensively tested, including for the shock tube in 1D, Rayleigh-Taylor instabilities in 2D and 3D (Stone et al. 2008). The initial conditions of the lightning are taken from the observations carried by Orville (1968b). To predict

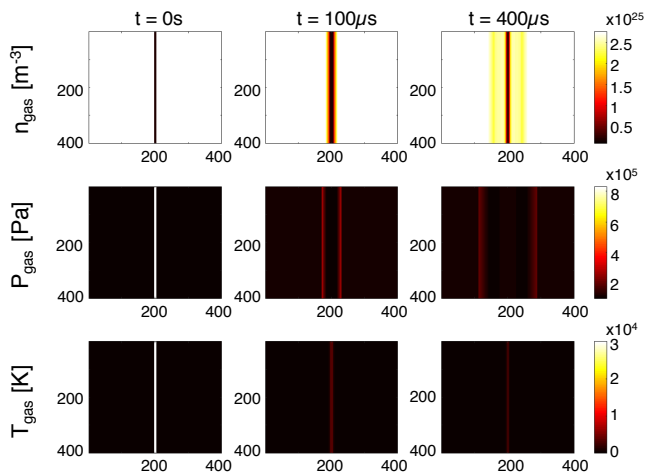


Figure 1. 2D snapshots of lightning shock wave propagation at 0s, 100 μ s, and 400 μ s. Spatial axis have units of cm. First row shows changes in the gas number density, second – in gas pressure, and third – in gas temperature.

the chemistry, we use the STAND2015 chemical network constructed for lightning shock chemistry along with the ARGO photochemistry/diffusion solver (Rimmer & Helling 2016), a Lagrangian solver that has recently been validated against the standard Eulerian solvers (Tsai et al. 2016). The chemical network solves for H/C/N/O chemistry and has been successfully benchmarked against both Contemporary and Early Earth models (Rimmer & Helling 2016). We apply these approaches to specific temperature profiles and bulk atmospheric compositions appropriate for the Early and Contemporary Earth.

2.1 Hydrodynamical shock modelling

We use ATHENA to set up a 2D hydrodynamical simulation of the shock waves propagation during the lightning. We explored a 1D and a 2D model setup which allowed us to demonstrate the stability of the hydrodynamic solution of our shock wave model. The 2D setup further allows for a first visualisation of the mainly 2D geometry of the lightning channel.

The computational grid contains 400x400 cells, each corresponding to 1 cm². The initial width of lightning channel is set to 1 grid cell. Two shock waves then propagate parallel in opposite directions, assuming open boundary conditions. For every point in time and space, ATHENA solves the equation of hydrodynamics (Appendix A). We assume that the cooling of the lightning channel occurs mainly due to radiative processes. Thus, we incorporate a radiative cooling function, discussed in Appendix B.

We assume the ideal gas with $\gamma = 1.44$. The initial conditions inside the lightning channel are set to $T_{in} = 30000$ K and $P_{in} = 8P_{gas}$ according to Orville (1968b). The lightning is initiated at 0 km altitude where the physical conditions of the air are the following: $P_{gas} = 103900$ Pa and $T_{gas} = 272.1$ K. The atmosphere is composed mostly of oxygen and nitrogen with traces of other elements, with the molar mass $M = 28.97$ mol g⁻¹. Figure 1 shows the changes in n_{gas} , P_{gas} , T_{gas} during the first 400 μ s.

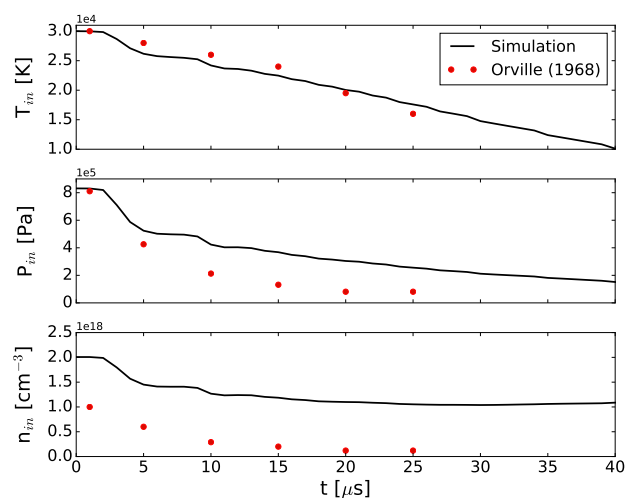


Figure 2. Temperature, T_{in} , pressure, P_{in} , and number density, n_{in} , profiles of the lightning in the first 40 μ s. Blue line – simulation results, red dots – Orville’s data. The deviation in number density values is a result of differences between our simulation and the estimate of Orville (1968c).

The P_{in} , n_{in} , T_{in} values are extracted from the centre of the initial discharge channel, i.e. from 200x200th grid cell, and are presented in the Figure 2. The simulation demonstrates a good fit with observational temperature data. Orville’s temperature values are believed to be precise and reliable since are obtained from NII emission line of multiple flash spectra. The number density curve obtained in the simulations show the difference with Orville’s by a factor of 2. Orville estimated the number density from H-alpha broadening due to Stark effect. Only one flash produced detectable spectral features, thus large errors are expected. The differences between simulation and observations is also observed in pressure curve. This is because our simulation explicitly respects the ideal gas law, whereas Orville estimates the pressure independently. The pressure values are taken from prior measurements of air at temperatures below 24000 K (Gilmore 1955), which is much lower than the estimated temperature inside the discharge channel.

All numerically obtained values of P , n , T never go to unreasonably low or high values, and the physical conditions of the medium return to pre-shocked values after 0.8 s. The simulation values of P , n , and T agree with ideal gas law, thus are considered and the $P_{in}(t)$, $n_{in}(t)$, $T_{in}(t)$ output is used as an input for chemical kinetics network.

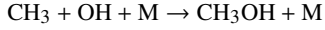
2.2 Chemical kinetics network

The lightning shock model is coupled to a 1D photochemistry-diffusion code ARGO (Rimmer & Helling 2016), which solves the continuity equations for vertical atmospheric chemistry:

$$\frac{\partial n_i}{\partial t} = P_i - L_i - \frac{\partial \Phi_i}{\partial z}, \quad (3)$$

where $n_i(t, z)$ [cm⁻³] is the number density of species i and $i = 1, \dots, N_s$, and N_s is the total number of species. P_i is the rate of production and L_i is the rate of loss, both with units

$\text{cm}^{-3} \text{ s}^{-1}$. The vertical change in flux, Φ_i , represents both Eddy and molecular diffusion. Except at one height in the atmosphere, this equation is solved precisely as described in Rimmer & Helling (2016), where each height has a constant gas temperature, T [K], and pressure, p [bar]. A parcel of gas is followed as it moves through the atmosphere, and chemistry is tracked for this parcel. The chemical network used here is the STAND2016 network (Rimmer & Helling 2016), except for R227/228:



for which we replace the rate coefficient used in Rimmer & Helling (2016) with the rate coefficient from Jasper et al. (2007), following Tsai et al. (2016).

Lightning shock chemistry is initiated deep in the atmosphere, where $p \sim 0.1\text{--}1$ bar. As discussed in Section 2.1, at a set height, $z_l = 0$ km, the lightning shock is initiated. Right when the parcel achieves this height, the lightning shock initiates. Pressure and temperature are determined in the manner described above in Section 2.1. The rate of change of these parameters, the magnitude of the temperature and the high pressures are such that any chemical timescale, or even the timescale for the lightning shock itself, is much shorter than the dynamical timescales. Although molecular diffusion is considered alongside the shock chemistry in the code, effectively, for the duration of the lightning shock, $\Phi_i = 0$.

Lightning achieves temperatures on the order of 30000 K at the beginning of our shock, and these temperatures will effectively dissociate and ionize the gas. To account for this without overly taxing the integrator, we set the initial conditions for the parcel at $z_l = 0$ km such that all species are fully dissociated and ionized. The elemental abundances are maintained, but entirely in the form of singly ionized cations. This initial condition deviates from our assumptions for the cooling rate (see Appendix B). For every cation, an electron, e^- , is introduced to preserve charge balance. This means that our assumed initial conditions are such that the degree of ionization, $f_e = 1$. This may seem artificial, but is not unreasonable if one considers that every collision in a 30000 K gas will be dissociating and/or ionizing. The barriers for dissociation and ionization are on the same order as the temperature, so the barrier will only slow things by at most a factor of $\sim \exp(20 \text{ eV} / kT) \sim 10^3$, for the highest ionization potentials. The time-scale for complete ionization in a 30000 K, 8 bar gas is therefore on the order of:

$$\frac{e^{-I/kT}}{\sigma v n_{\text{gas}}} \approx 10^{-9} \text{ s.}$$

This is vastly shorter than the time resolution in which we consider our lightning shock. After the temperature falls to ~ 10000 K, however, chemical timescales extend to the length of seconds, and at much lower temperatures, potentially to days or years. In this manner, lightning chemistry can linger for an extended period of time and can affect the entire atmospheric chemistry above which lightning has recently been initiated.

The competition between the rate of lightning events and the chemical time-scales, largely set by the pressures and the energetic barriers for destroying species generated in the lightning shock at quantities far outside equilibrium, will determine the global mixing ratios of lightning species. This

sort of analysis would require detailed lightning statistics, of the form of, e.g. Hodosán et al. (2016b). As a first step, we do not consider this detailed statistics, but rather assume every parcel of gas at the exoplanetary surface receives a lightning shock.

A parcel experiences the shock at $z = 0$ km, and remains at this height for a time set by the dynamical timescale, t_d [s]. The dynamical timescale is determined from the Eddy Diffusion coefficient, K_{zz} [$\text{cm}^2 \text{ s}^{-1}$] and the difference between the heights at which the constant temperatures and pressures are set, Δh [km], as follows:

$$t_d = \frac{(\Delta h)^2}{K_{zz}} \quad (4)$$

At $z = 0$, $K_{zz} = 10^5 \text{ cm}^2 \text{ s}^{-1}$ and $\Delta h = 2$ km, so $t_d \approx 4.6$ days. Therefore, the parcel receives the shock, remains at $z = 0$ km for 4.6 days, and then moves up to a new height. Right before the parcel is moved, its chemistry is recorded, and the entire region at $z = 0$ km is treated as having the final chemistry of this parcel. This is effectively setting the time between each lightning event that the gas at $z = 0$ km experiences equal to 4.6 days. From this timescale and the average energy of a lightning flash, we can work out the effective lightning density assumed for our model.

The flash density, ρ_{fl} [flashes $\text{km}^{-2} \text{ h}^{-1}$] will be proportional to the number density of the gas at the shock n_{in} [cm^{-3}] multiplied by the energy added to each particle by the shock, which by the equipartition theorem we will set to $3/2 k_B \Delta T \approx 3/2 k_B T_{\text{in}}$. Treating this as an ideal gas:

$$\rho_{\text{fl}} = \Delta h \frac{P_{\text{in}}}{k_B T_{\text{in}}} \frac{\frac{3}{2} k_B T_{\text{in}}}{E_{\text{fl}}} \frac{K_{zz}}{(\Delta h)^2}, \quad (5)$$

$$= \frac{3 P_{\text{in}} K_{zz}}{2 \Delta h E_{\text{fl}}}, \quad (6)$$

where we take $E_{\text{fl}} = 4 \times 10^8 \text{ J}$ as the average energy of a lightning flash (Borucki & Chameides 1984). This provides a value of $\rho_{\text{fl}} \approx 5.4 \times 10^4 \text{ flashes km}^{-2} \text{ h}^{-1}$. By comparison, the highest flash density observed on Earth is $\sim 0.1 \text{ flashes km}^{-2} \text{ h}^{-1}$ produced in thunderstorms in Florida and other areas in the United States (Huffines & Orville 1999). We consider these intense lightning flash densities to be a practical upper limit for estimating the chemical impact of lightning on Earth-like exoplanets with Earth-like flash energies.

2.3 Initial conditions

To study the impact of lightning on the atmospheric chemistry, we firstly assume that the pressure and temperature profiles of both Contemporary and Early Earth are identical, consistent with Rimmer & Helling (2016). The temperature profile of the Earth atmosphere is adapted from Hedin (1987, 1991) as shown in Figure 3.

The chemical composition of present-day Earth is oxidising, dominated by nitrogen (80%) and oxygen (20%) with traces of other elements. The chemical abundances at 0 km altitude (1 atm) are summarised in Table 1 and are chosen according to Seinfeld & Pandis (2016).

For Early Earth, we adapt the the atmospheric composition introduced by Kasting (1993). His weakly reducing atmosphere is the best simultaneous explanation of the observed hydrogen fractionation, $^{22}\text{Ne}/^{20}\text{Ne}$ and xenon isotope

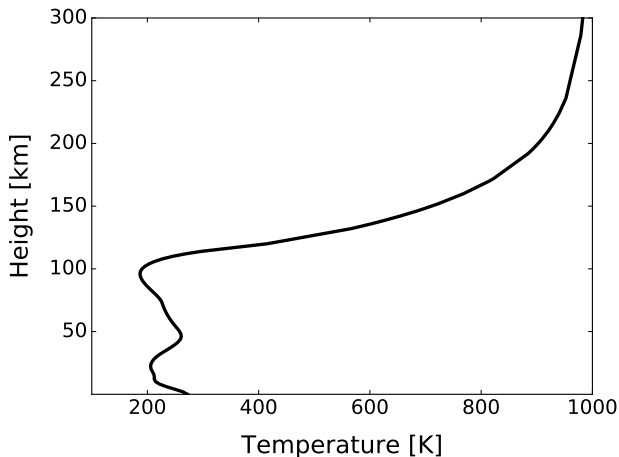


Figure 3. Temperature profile of Earth (Hedin 1987, 1991).

Table 1. Chemistry at the surface of the Contemporary and Early Earth used in our models.

Chemical species	Contemporary Earth	Early Earth
N ₂	0.8	0.8
O ₂	0.2	0.0
H ₂ O	0.01	0.01
CO ₂	$3.5 \cdot 10^{-4}$	0.1
CH ₄	$2.0 \cdot 10^{-6}$	0.0
H ₂	$1.0 \cdot 10^{-6}$	$1.0 \cdot 10^{-3}$
CO	$6.0 \cdot 10^{-7}$	$5.0 \cdot 10^{-5}$
N ₂ O	$6.0 \cdot 10^{-7}$	0.0
O ₃	$2.0 \cdot 10^{-8}$	0.0
HNO ₃	$1.0 \cdot 10^{-10}$	0.0
NO ₂	$6.0 \cdot 10^{-11}$	0.0
NO	$2.5 \cdot 10^{-11}$	0.0
HO ₂	$7.233 \cdot 10^{-12}$	0.0
HO	$7.2333 \cdot 10^{-14}$	0.0

ratios (Hunten 1973; Ozima & Nakazawa 1980; Zahnle et al. 1990; Zahnle 1990), and is the atmosphere that is most consistent with the best understood atmospheric escape rates of H₂ (Lammer et al. 2008). According to Kasting (1993), the atmosphere of Early Earth is assumed to consist mostly of 80% of N₂ and 10% of CO₂, with traces of H₂O, H₂, and CO at 0 km altitude; see Table 1.

The cooling function for both atmospheres is estimated as described in Appendix B for the main chemical constituents – N₂ and O₂ for Contemporary Earth, and N₂ and CO₂ for Early Earth.

3 RESULTS

We use the model discussed earlier to study the practical upper limit of the impact of lightning on present-day and Early Earth atmospheres. The results provide an estimated impact of global super-intense lightning storms on exoplanets similar to Earth and orbiting Sun-like stars. The model also allows us to predict the results of balloon experiments within lightning storms on the Contemporary Earth. In addition, it can be used as a tool for estimating the chemical impact of lightning on the Early Earth.

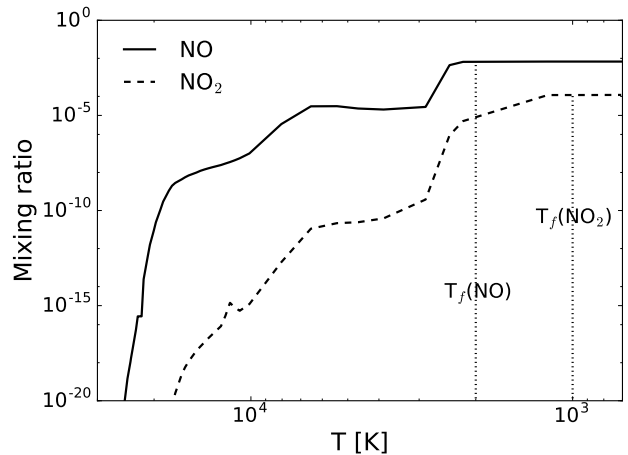


Figure 4. Mixing ratios of NO (solid line) and NO₂ (dashed line) as a function of temperature during lightning for the Contemporary Earth. The mixing ratios reach up to $X(\text{NO}) = 6.766 \cdot 10^{-3}$ and $X(\text{NO}_2) = 1.175 \cdot 10^{-4}$. The estimates 'freeze-out' temperature are shown in grey dotted line, $T_f(\text{NO}) \approx 2000 \text{ K}$ and $T_f(\text{NO}_2) \approx 1000 \text{ K}$.

3.1 Contemporary Earth

We first turn our attention to the NO_x production during lightning in order to validate the chemical output of the code. At high temperatures nitric oxide is formed via Zel'dovich reactions 7 and 8.



STAND contains the reverse reaction of Reaction (8):



The reverse reaction rates will lead the gas into chemical equilibrium if enough time is given and if no disequilibrium processes (eg. photochemistry) are included. Such reaction rates are not always physically accurate, and in our case lead to significant underestimation for reaction 8 at high temperatures. Thus it was decided to use experimentally obtained coefficients from Michael & Lim (1992) at high temperatures to calculate the rate coefficient, k [cm³ s⁻¹], via equation 10 where T [K] is the temperature:

$$k(T) = 1.66 \cdot 10^{-10} \text{ cm}^3 \text{ s}^{-1} e^{-3.8 \cdot 10^4 \text{ K}/T}. \quad (10)$$

This clearly demonstrates the need for experimental studies that would provide the lacking rate coefficients for this and other missing reactions. Our model shows that Zel'dovich reactions take place only in the temperature range $\approx 2000 - 10100 \text{ K}$. The rate of formation of NO reaches up to $\approx 10^{20} \text{ cm}^{-3} \text{ s}^{-1}$.

Another 3-body reaction is consistently observed to produce nitric oxide from the very beginning of the electric discharge, and is:



where M is any third body. This reaction disappears only when the heated air returns into thermodynamic equilibrium and cools down to pre-shocked temperatures. The importance of this 3-body association (Eq. 11) to forming NO

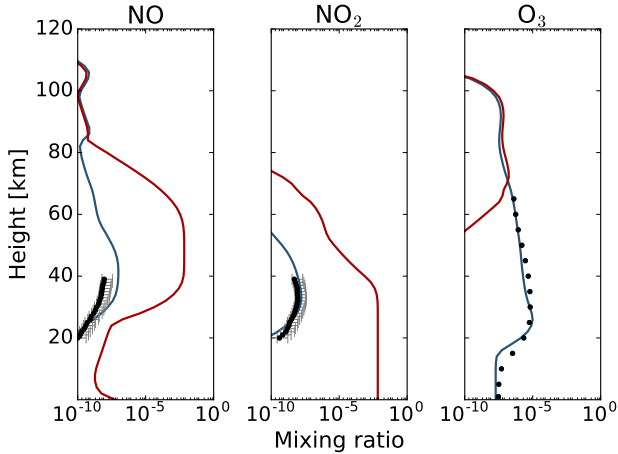


Figure 5. The atmospheric profiles of NO, NO₂, and O₃ for the Contemporary Earth. Red line – with lightning, blue line – without, black dots – balloon observations (NO and NO₂ from Sen et al. (1998), O₃ from Massie & Hunten (1981)). The model demonstrates a good fit with the measurements.

during a lightning event has not to our knowledge been mentioned anywhere in the literature before now.

Figure 4 demonstrates the change in mixing ratios² during the lightning for both NO (solid line) and NO₂ (dashed line). This allows to estimate the ‘freeze-out’ temperature, T_f , after which almost no change in the mixing ratios occur (vertical dashed line) (Navarro-González et al. 2001). For NO, $T_f(\text{NO})$ is estimated to be $\approx 2000 \pm 500$ K. The net yield is calculated from our results using Eq. (49) from Rimmer & Helling (2016), and is equal to $P(\text{NO}) = (8.04 \pm 2.00) \cdot 10^{16}$ molecules J^{-1} . Borucki & Chameides (1984) predicted the net yield of produced nitric oxide during the lightning discharge to be $(9 \pm 2) \cdot 10^{16}$ molecule J^{-1} . The laboratory studies of electric discharge demonstrated the yield of $(1.5 \pm 0.5) \cdot 10^{17}$ molecule J^{-1} (Navarro-González et al. 2001). The produced levels of NO are in agreement with both experimental and observational values.

The atmospheric profiles for each chemical specie are produced by the model and include the photochemical and diffusion processes. Figure 5 shows the profiles of NO, NO₂, and O₃ in the case of lightning (red) and without (blue). The initial increase of NO and NO₂ is a consequence of lightning at 0 km altitude, where the mixing ratios reach $X(\text{NO}) = 4.9 \cdot 10^{-8}$ and $X(\text{NO}_2) = 7.3 \cdot 10^{-3}$. Nitric oxide is then destroyed to produce NO₂, NO₃, and N₂O₃. At 10–60 km altitude, the abundance of NO is increasing due to the reverse reactions reaching the maximal value of $X(\text{NO}) = 6.5 \cdot 10^{-3}$. NO₂ remains constant until 40 km. Higher in the atmosphere, the photochemical reactions destroy both NO and NO₂.

The fraction of ozone is visibly reduced by the lightning because most of the oxygen is in the nitric oxide. When the photochemical destruction of NO becomes efficient, the mixing ratio of O₃ reaches its non-lightning value and even slightly exceeds it, reaching $X(\text{O}_3) = 1.9 \cdot 10^{-7}$ at 75 km.

² The mixing ratio of a species X is the number density of that species divided by the total number density: $n(X)/n_{\text{tot}}$.

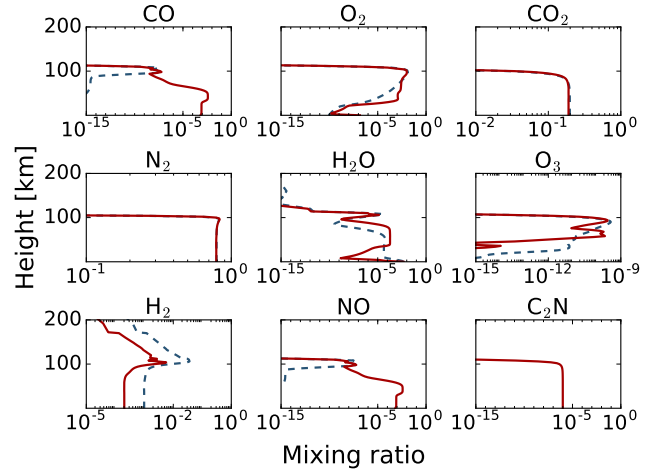


Figure 6. Atmospheric profiles of CO, O₂, CO₂, N₂, H₂O, O₃, H₂, NO, and C₂N for the Early Earth. Blue line – lightning off, red line – with lightning on.

The atmospheric profiles in Fig. 5 also include the values obtained during the balloon measurements when no lightning is present in the atmosphere. The simulation results are in a good agreement with the measurements. Thus, we can use the results to predict maximal mixing ratios for balloon measurements taking place from within a lightning storm.

3.2 Early Earth

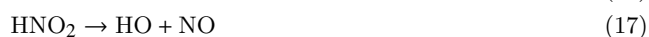
We then apply our code to the Early Earth by shocking our parcel at 0 km height within a bulk atmosphere from Rimmer & Helling (2016). We assume an effective lightning flash density of 5.4×10^4 flashes $\text{km}^{-2} \text{h}^{-1}$. Figure 6 shows the variations in atmospheric profiles of the main chemical elements for both with and without lightning.

The abundance of N₂ and CO₂ decrease by a very small amount during the lightning discharge. The mixing ratio of CO increases initially to 10^{-2} and remains constant until gets dissociated by photochemistry. The net amount of H₂ is decreased by the presence of lightning. This correlates with the production of H-containing molecules during electric discharge, such as HNO, NH₂OH.

Similar to the present-day Earth case, the simulation demonstrates very efficient formation of nitric oxide during the lightning event. The maximal mixing ratio during electric discharge reaches up to $X(\text{NO}) = 1.33 \cdot 10^{-3}$. The ‘freeze-out’ temperature is approximated to be 2190 ± 300 K. Thus, using Eq. (49) from Rimmer & Helling (2016), the estimated yield is $P(\text{NO}) \approx 1.42 \pm 0.19 \cdot 10^{16}$ J^{-1} . Kasting & Walker (1981) estimated the production efficiency during the lightning event in the Early Earth as $(0.27-1.1) \cdot 10^{16}$ molecule J^{-1} , assuming the ‘freeze-out’ temperature to equal 3500 K. The difference in ‘freeze-out’ temperatures for Contemporary and Early Earth atmospheres arise due to the different cooling rates appropriate for the bulk composition of Early Earth. Such a large yield makes both NO and NO₂ possible candidate for the lightning tracer on any Earth-like planet around any star. However, stars with different XUV field will destroy some of these species more or less rapidly.

The computational model shows that different reactions

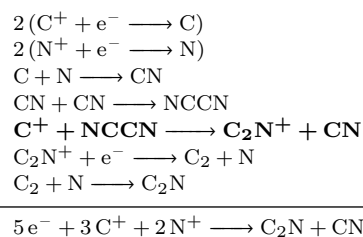
are responsible for NO formation compared to the Contemporary Earth atmosphere. Zel'dovich reactions are present, however, reaction 13 occurs only in the narrow temperature range from $\approx 3000 - 2400$ K. This is explained by the overall reduced amount of oxygen present in Early Earth atmosphere. The 3-body reaction is present from the beginning of the lightning and disappears at ≈ 2400 K. At temperatures lower than 2000 K, nitric oxide is formed due to the dissociation of more complex H-rich molecules produced by the lightning, such as NHO, NH₂O, and HNO₂ (reactions 15, 16, and 17).



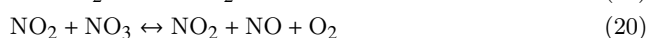
The noticeable deviation from the non-lightning case is also observed in the profile of C₂N. The mixing ratio reaches $1.1 \cdot 10^{-6}$ during the lightning and remains constant up until 100 km. In reality, the destruction of C₂N might occur at much lower altitudes in the atmosphere, since this molecule has not been studied in detail experimentally. However, there have been extensive theoretical studies into its reactions with H₂O, CH₄, NH₃, C₂H₂ (Wang et al. 2006) and H₂S (Dong et al. 2010). These theoretical studies suggest that reactions between C₂N and these species proceed without barriers, but the branching ratios and rate coefficients remain undetermined. There has been some yet unpublished work involving the reaction of C₂N with CO₂, which is expected to encounter a moderate barrier, and with NO₂, which may be proceed efficiently (J. Wang, private communication). Because the rate constants for these reactions remain undetermined, STAND at present does not include these destruction pathways for C₂N. We are hopeful that future work will be performed to fix the branching ratios and allow us to estimate reliable rate constants for these destruction pathways, in order to determine both the stability of C₂N within the deep atmosphere, as well as the chemical fate of its products. The 'freeze-out' temperature for C₂N, sans the destruction pathways, is estimated to be around 4000 K. The formation path from a fully ionised gas is determined shown in Table 2. The reaction in bold corresponds to the rate-limiting step which defines the timescales for the whole reaction chain. We have found no literature relating cyanomethylidyne (C₂N) either to lightning or to atmospheric chemistry, although Wang et al. (2006), among other publications, propose that C₂N would plausibly be present in detectable quantities within interstellar clouds and disks. Study of the reaction kinetics of C₂N is important for all hydrogen-poor atmospheres where dissociation is important. It doesn't matter whether the dissociation is caused by lightning or geochemistry or biochemistry.

Lightning causes the molecular oxygen to decrease initially since oxygen atoms are more likely to end up in the nitric oxide. Higher in the atmosphere, the fraction of O₂

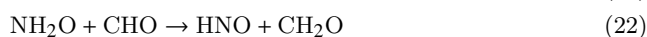
Table 2. Balanced path for C₂N formation during the lightning. The reaction in bold corresponds to the rate-limiting step.



increases due to the dissociation of NO_x molecules:



In the non-lightning case, oxygen forms from hydrogen and carbon containing reactions. These reactions are not observed when the lightning is present. Only reactions involving NO_x produce substantial amount up to 100 km. At 24 km, a rapid decrease in the mixing ratio of O₂ is caused by the interactions involving nitrosyl hydride (HNO). HNO is formed from the following reactions involving NH₂O, and destroys molecular oxygen in the following way:



The NH₂O is a highly unstable, transitional species of known importance in many chemical kinetics pathways, and is efficiently formed by lightning. It quickly reacts away to nitrosyl hydride (HNO) which then is destroyed via oxidation, resulting in a significant decrease of molecular oxygen.

4 TRANSMISSION SPECTROSCOPY WITH LIGHTNING

Synthetic transmission spectra in the range of 0.5 - 10 μm were computed for an Earth like planet orbiting a Sun-like star. Four models were computed for the "Early Earth" and "Contemporary Earth" scenarios, with and without lightning. The 1D radiative transfer forward model of the Tau-REx atmospheric retrieval framework (Waldmann et al. 2015a,b), based on the Tau code by Hollis et al. (2013), was adapted to compute the transmission spectrum given the variable temperature-pressure profiles and altitude dependent mixing ratios by the STAND network. The transmission spectra are given in terms of the ratio of the radius of the planet, R_p to the radius of the star R_* squared, or $R_p^2/(R_*)^2$, and scaled by 10^{-5} so that the features can be seen by eye.

Due to the large number of possible opacities of the chemical network, we restricted the computation of the transmission spectra to the most prominent species: O₂, O₃, NO, NO₂, NH₃, HCOOH, HCN, H₂O, CO₂, CO, CH₄, C₂H₂ and C₂H₆. The mean molecular weight of the atmosphere was calculated using the full chemical network. Temperature and pressure broadened absorption cross-sections were computed at a constant spectral resolution of 7000 and binned

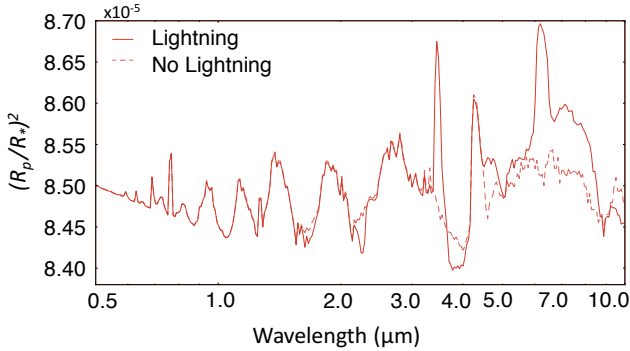


Figure 7. Transmission spectrum of a Contemporary-Earth-like planet 1 AU from a solar-type star, in terms of the transit depth versus the wavelength in microns.

to 100 as shown in Figures 7 and 8. Molecular line list opacities were obtained from the ExoMol project (Tennyson & Yurchenko 2012), HITRAN (Rothman et al. 2009, 2013) and HITEMP (Rothman et al. 2010). Rayleigh scattering and collision induced absorption of $\text{H}_2\text{-H}_2$ and $\text{H}_2\text{-He}$ (Richard et al. 2012) were also included. The atmospheres are assumed to be cloud-free. Molecular contributions to the opacity for the “Modern-Earth” scenario, both with and without lightning, are shown in Figure 9.

Figure 9 shows the major contributors of molecular opacity for the Contemporary Earth. The effect lightning has on the spectrum of the Early Earth comes from the same molecular sources as the dominant features. These are NO and NO_2 , CO and CO_2 and O_2 . Although lightning efficiently destroys ozone, it does so in a region where the ozone features are collisionally broadened. The difference in O_3 opacity changes the transit depth by less than 10^{-8} . Some differences in the absorption are present around $4 \mu\text{m}$, affecting the transit depth by a factor of 5×10^{-7} , and CO absorbs with similar efficiency around $4.5 \mu\text{m}$. The largest effect on the opacity due to nitrogen dioxide (NO_2).

Nitrogen dioxide is an efficient absorber at wavelengths of $\sim 3.4 \mu\text{m}$ and $\sim 6.2 \mu\text{m}$, and increases the transit depth at these wavelengths by at most 2 ppm ($1 \text{ ppm} = 10^{-6}$). Even with several hours of observation, the James Webb Space Telescope will only be able to resolve changes in transit depth on the order of 10 ppm (Deming et al. 2009), and would need to compete with instrumental systematics and stellar features far larger than the signal itself (Barstow et al. 2015). Detection of the chemical impact of lightning on Earth-like planets, even for the most extreme planet-wide storms (such as Earth-like versions of those discussed by Hodosán et al. 2016a), will have to wait for the next generation of telescopes, such as the ELT (Gilmozzi & Spyromilio 2008). Although the $6.2 \mu\text{m}$ feature will be obscured by the atmosphere, the $\sim 3.4 \mu\text{m}$ feature lies roughly within an atmospheric window, and could be observable from the ground with this kind of future instrumentation. It would then be important to determine what effects reducing the scale of the lightning storm would have on these spectral features, and whether these features would be at all detectable with future instrumentation for more Earth-like thunderstorms.

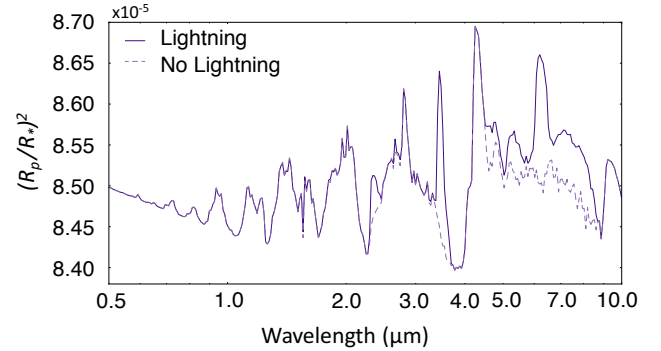


Figure 8. Transmission spectrum of an Early-Earth-like planet 1 AU from a young solar-type star, in terms of the transit depth versus the wavelength in microns.

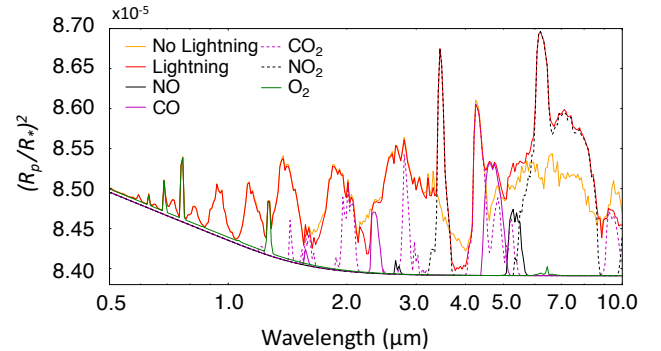


Figure 9. Molecular contributions for the Contemporary Earth transmission spectrum, as a function of wavelength [μm].

5 CONCLUSIONS

We have created the model that can be used to study the impact of lightning for a variety of exoplanetary atmospheres that differ both physically and chemically. We apply this model to an Earth-like rocky exoplanet with both the bulk composition of the Contemporary Earth (N_2 and O_2) and the Early Earth (N_2 and CO_2). We compare our results for the Contemporary Earth, and find that our predictions agree with the experimental and observational yields of NO and NO_2 from lightning. We also make predictions for lightning-induced chemical profiles of NO, NO_2 and O_3 within thunder clouds.

We show that NO is efficiently formed during the lightning via Zel’dovich reactions at temperatures below 10000 K. The studies of Contemporary Earth atmosphere showed, that the considerable contribution to the nitric oxide formation is made by a 3-body reaction 11. This reaction is present from the very beginning of the lightning. No information has been found in the literature relating this three-body association to the electric discharge.

For the Early Earth, we find also an enhancement in NO and NO_2 , as well as CO. The destruction of O_3 by lightning is not as important for the Early Earth because comparatively very little O_3 is predicted within this atmosphere to begin with. We predict also a large production of cyanomethyldyne (C_2N), a species which is also predicted to be present within the interstellar medium. Wang et al.

(2006) and others have calculated various reaction pathways for C₂N, but thus far no reliable rate constants or branching ratios have been published for these reactions. C₂N is sufficiently abundant to potentially have an important impact on the atmosphere, either as a spectral signature of lightning, or via the products of its destruction. Further laboratory and theoretical work on this species will be necessary to determine its fate.

Finally, we explored the effect of these species on hypothetical transmission spectra for rocky planets of Earth size with these model atmospheres. Providing an extreme case for the flash density, and therefore chemical yield, we found that, for rocky planets with global and very active lightning storms, the spectrum changes substantially at 3.4 μm and 6.2 μm , but these differences are too small to be plausibly detected with JWST, and will have to wait for a future generation of telescopes. Thus, implementation of more physical lightning flash densities will only reduce the already small effect, and will not be relevant for observers unless lightning energetics is very different on other rocky exoplanets than on Earth. The observed spectra will also depend on the composition of clouds which are not included in the model. Incorporation of lightning event rates and clouds can be the next steps for the proper spectra estimation. In the meantime, the tool we have developed for the exoplanet community can be applied to the atmospheres of both hot and cold Jupiters, Brown Dwarfs and mini-Neptunes. If the variability due to lightning is of the same order as the magnitude of the spectral features, as we predict for rocky exoplanets, features of global lightning storms may be observable in these objects.

ACKNOWLEDGEMENTS

AA, PBR and ChH gratefully acknowledge the support of the ERC Starting Grant #257431. IW, MR, SNY and JT also gratefully acknowledge the support of the STFC (ST/K502406/1), and the ERC projects ExoMol (26719) and ExoLights (617119). PBR thanks John Sutherland and Y.-H. Ding for helpful comments about the chemistry.

REFERENCES

- Anglada-Escudé G., et al., 2016, *Nature*, 536, 437
 Barstow J. K., Aigrain S., Irwin P. G. J., Kendrew S., Fletcher L. N., 2015, *MNRAS*, 448, 2546
 Bean J. L., Miller-Ricci Kempton E., Homeier D., 2010, *Nature*, 468, 669
 Beasley W., Uman M. A., Rustan Jr. P. L., 1982, *J. Geophys. Res.*, 87, 4883
 Borucki W. J., Chameides W. L., 1984, *Rev. Geophys.*, 22, 363
 Deming D., et al., 2009, *PASP*, 121, 952
 Dong X., Wang L., Tian Y., 2010, *J. Mol. Struct.: THEOCHEM*, 947, 45
 Dressing C. D., et al., 2013, *ApJ*, 767, 95
 Frost D. C., McDowell C. A., 1956, *Proc. R. Soc. A*, 236, 278
 Gillon M., et al., 2016, *Nature*, 533, 221
 Gillon M., et al., 2017, *Nature*, 542, 456
 Gilmore F. R., 1955, CA: RAND Corporation
 Gilmozzi R., Spyromilio J., 2008, in *Ground-based and Airborne Telescopes II*. p. 701219, doi:10.1117/12.790801
 Hedin A. E., 1987, *J. Geophys. Res.*, 92, 4649
 Hedin A. E., 1991, *J. Geophys. Res.: Space Phys.*, 96, 1159
 Helling C., et al., 2016, *Surv. Geophys.*, 37, 705
 Hodosán G., Rimmer P. B., Helling C., 2016a, *MNRAS*, 461, 1222
 Hodosán G., Helling C., Asensio-Torres R., Vorgul I., Rimmer P. B., 2016b, *MNRAS*, 461, 3927
 Hollis M. D. J., Tessenyi M., Tinetti G., 2013, *Comp. Phys. Comm.*, 184, 2351
 Huffines G. R., Orville R. E., 1999, *Journal of Applied Meteorology*, 38, 1013
 Hunten D. M., 1973, *J. Atmos. Sci.*, 30, 1481
 Jasper A. W., Klippenstein S. J., Harding L. B., Ruscic B., 2007, *Journal of Physical Chemistry A*, 111, 3932
 Jebens D. S., Lakkaraju H. S., McKay C. P., Borucki W. J., 1992, *Geophys. Res. Lett.*, 19, 273
 Kane S. R., et al., 2016, *ApJ*, 830, 1
 Kasting J., 1993, *Science*, 259, 920
 Kasting J. F., Walker J. C. G., 1981, *J. Geophys. Res.*, 86, 1147
 Kreidberg L., Loeb A., 2016, arXiv preprint arXiv:1608.07345
 Lammer H., Kasting J. F., Chassefière E., Johnson R. E., Kulikov Y. N., Tian F., 2008, *Space Sci. Rev.*, 139, 399
 Massie S. T., Hunten D. M., 1981, *J. Geophys. Res.*, 86, 9859
 Michael J. V., Lim K. P., 1992, *J. Chem. Phys.*, 97, 3228
 Miller S. L., 1953, *Science*, 117, 528
 Navarro-González R., Villagrán-Muniz M., Sobral H., Molina L. T., Molina M. J., 2001, *Geophys. Res. Lett.*, 28, 3867
 Orville R. E., 1968a, *J. Atmos. Sci.*, 25, 827
 Orville R. E., 1968b, *J. Atmos. Sci.*, 25, 839
 Orville R. E., 1968c, *J. Atmos. Sci.*, 25, 852
 Ozima M., Nakazawa K., 1980, *Nature*, 284, 313
 Post D., Jensen R., Tarter C., Grasberger W., Lokke W., 1977, *Atomic Data and Nuclear Data Tables*, 20, 397
 Price C., Penner J., Prather M., 1997, *J. Geophys. Res.: Atmos.*, 102, 5929
 Radigan J., Jayawardhana R., Lafrenière D., Artigau É., Marley M., Saumon D., 2012, *ApJ*, 750, 105
 Richard C., et al., 2012, *Journal of Quantitative Spectroscopy & Radiative Transfer*, 113, 1276
 Rimmer P. B., Helling C., 2016, *ApJS*, 224, 9
 Rothman L. S., et al., 2009, *J. Quant. Spectrosc. Radiative Transfer*, 110, 533
 Rothman L. S., et al., 2010, *J. Quant. Spectrosc. Radiative Transfer*, 111, 2139
 Rothman L. S., et al., 2013, *J. Quant. Spectrosc. Radiative Transfer*, 130, 4
 Rugheimer S., Kaltenecker L., Zsom A., Segura A., Sasselov D., 2013, *Astrobiology*, 13, 251
 Seinfeld J. H., Pandis S. N., 2016, *Atmospheric chemistry and physics: from air pollution to climate change*. John Wiley & Sons
 Sen B., Toon G. C., Osterman G. B., Blavier J.-F., Margitan J. J., Salawitch R. J., Yue G. K., 1998, *J. Geophys. Res.: Atmos.*, 103, 3571
 Sing D. K., et al., 2011, *MNRAS*, 416, 1443
 Stone J. M., Gardiner T. A., Teuben P., Hawley J. F., Simon J. B., 2008, *ApJS*, 178, 137
 Tennyson J., Yurchenko S. N., 2012, *MNRAS*, 425, 21
 Tsai S.-M., Lyons J. R., Grosheintz L., Rimmer P. B., Kitzmann D., Heng K., 2016, arXiv preprint arXiv:1607.00409
 Waldmann I. P., Tinetti G., Rocchetto M., Barton E. J., Yurchenko S. N., Tennyson J., 2015a, *ApJ*, 802, 107
 Waldmann I. P., Rocchetto M., Tinetti G., Barton E. J., Yurchenko S. N., Tennyson J., 2015b, *ApJ*, 813, 13
 Wang J., Ding Y.-h., Sun C.-c., 2006, *ChemPhysChem*, 7, 710
 Woitke P., Krueger D., Sedlmayr E., 1996, *A&A*, 311, 927
 Wordsworth R. D., Forget F., Selsis F., Millour E., Charnay B., Madeleine J.-B., 2011, *ApJ*, 733, L48
 Yang J., Cowan N. B., Abbot D. S., 2013, *ApJ*, 771, L45
 Zahnle K. J., 1990, *Geo. Soc. Am. Special Papers*, 247, 271
 Zahnle K., Kasting J. F., Pollack J. B., 1990, *Icarus*, 84, 502

Zel'dovich Y. B., Raizer Y. P., 2002, *Physics of Shock Waves and High-Temperature Hydrodynamic Phenomena*. Dover Books on Physics, Dover Publications
 de Wit J., et al., 2016, *Nature*, 537, 69

APPENDIX A: EQUATIONS OF CONTINUITY

ATHENA solves the equations of hydrodynamics, including a cooling term, and the equation of state A4. Hydrodynamics equations respect a principle of mass A1, momentum A2, and energy A3 conservation, where ρ – mass density [kg m⁻³], \mathbf{v} – velocity vector [m/s], P – pressure [Pa], E – total energy [J], γ – ratio of heat capacities, and Λ – radiative cooling function [J m⁻³ s⁻¹] (see Appendix) (Stone et al. 2008).

$$\frac{\partial \rho}{\partial t} + \nabla \cdot [\rho \mathbf{v}] = 0 \quad (\text{A1})$$

$$\frac{\partial (\rho \mathbf{v})}{\partial t} + \nabla \cdot [\rho \mathbf{v} \mathbf{v} + P] = 0 \quad (\text{A2})$$

$$\frac{\partial E}{\partial t} + \nabla \cdot [(E + P)\mathbf{v}] = -\rho^2 \Lambda \quad (\text{A3})$$

$$E = \frac{P}{\gamma - 1} + \frac{\rho(\mathbf{v} \cdot \mathbf{v})}{2} \quad (\text{A4})$$

APPENDIX B: RADIATIVE COOLING

The temperature dependence of lightning shocks is predominately due to radiative cooling. If not for radiative cooling, the time-scale for the temperature to decrease from ~ 30000 K to ~ 10000 K would be on the order of seconds, rather than microseconds. Predicting accurate cooling rates ab initio would depend on detailed microphysics for various compositions at temperatures and densities not yet investigated, and would require a fully coupled and self-consistent lightning chemistry and radiative hydrodynamics model, which is beyond present computational capabilities.

For this paper, we instead take a phenomenological approach to the radiative cooling function, appropriate for a high density high temperature plasma resulting from the lightning shock. We take a low-density approximation as our leading term and then add higher order correction terms to account for the high plasma density that exists within a lightning shock.

As explained above (Section 1), at the initial temperature of 30000 K for the centre of the lightning shock, we assume an artificial initial state where all molecules have completely dissociated away, and all remaining atoms are ionised. Collisional ionisation dominates, and to second order, is balanced by the total recombination rate, satisfying the conditions for “coronal equilibrium”. In effect, the leading term is obtained under the assumption that every excitation is collisional and not due to reabsorbing emitted light, and that radiative, rather than collisional, de-excitation dominates. We therefore use the parametrised cooling functions of Post et al. (1977), which account for

free-free emission, emission from (bound-free) radiative recombination and cooling from line (bound-bound) emission.

The second order cooling rates, Λ_1 [cm³ s⁻¹] are given for a single species X by the polynomial:

$$\log_{10} \Lambda_2(X) = \sum_{i=0}^5 A_i(X) t^i, \quad (\text{B1})$$

where $t = \log_{10} [T_e/(1 \text{ keV})]$ and T_e [keV] is the electron temperature. For multiple species, we sum the mixing ratios of that species, remembering that every constituent in the atmosphere is completely dissociated into its atomic form and then ionized, such that the entire gas is comprised of electrons and cations. The volume mixing ratio is represented for cationic species X by $x(X) = n(X)/n_{\text{cat}}$ where $n(X)$ [cm⁻³] is the number density of the cation and n_{cat} [cm⁻³] is the sum of all cations in the gas: $n_{\text{cat}} + n(e^-) = n_{\text{tot}}$. For our purposes, we consider the gas to be comprised of cations from the three atoms C, N and O. Therefore, the Eq.(B1) for each species is weighted by its cationic mixing ratio and then summed:

$$\begin{aligned} \Lambda_2 &= \sum_{i=0}^5 x(\text{C}) A_i(\text{C}) t^i + \sum_{i=0}^5 x(\text{N}) A_i(\text{N}) t^i + \sum_{i=0}^5 x(\text{O}) A_i(\text{O}) t^i, \\ &= \sum_{i=0}^5 [x(\text{C}) A_i(\text{C}) + x(\text{N}) A_i(\text{N}) + x(\text{O}) A_i(\text{O})] t^i. \end{aligned} \quad (\text{B2})$$

These values in the brackets can be represented by a single coefficient relevant for the atmosphere in question, B_i , such that:

$$\begin{aligned} \log_{10} \Lambda_2 &= \sum_{i=0}^5 B_i t^i, \\ B_i &= x(\text{C}) A_i(\text{C}) + x(\text{N}) A_i(\text{N}) + x(\text{O}) A_i(\text{O}). \end{aligned} \quad (\text{B3})$$

The values we use for B_i can be found in B1.

At low enough densities, this leading order term, Λ_2 , dominates. Above a certain critical density, n_c [cm⁻³], collisional cooling becomes important as well as re-absorption of emitted energy. The medium ceases to become transparent to its own radiation. We simply take the critical cooling rate suggested by the upper limit of Post et al. (1977), $n_c = 10^{16}$ cm⁻³. By analogy to many-body chemical reactions, we modify the cooling term as follows:

$$\Lambda = \frac{\Lambda_2}{1 + \sum_{k=1}^{k_{\text{max}}} \left(\frac{n}{n_c}\right)^k}. \quad (\text{B4})$$

The number of terms to be summed, the value of k_{max} , would be set by the detailed microphysics. This would take the form of temperature and pressure-dependent higher order cooling rates. Additionally, as the gas cools, eventually atoms react to form complex molecules. These molecules will have different cooling rates than the atoms.

Recalling that our method is phenomenological, we set k_{max} to whatever value reproduces the temperature observations from Orville (1968b). Testing values from 1 to 10, we found that $k_{\text{max}} = 6$ best reproduces the observed temperature dependence. Cooling rates for different values of k_{max} are shown in Figure X. The quality of the fit with $k_{\text{max}} = 6$ is shown in Figure 2. The dependency of the cooling rate on density in Eq. (B4) agrees with the density dependence found in rigorous microphysical investigations into cooling

Table B1. A_i Coefficients and Mixing Ratios for the Cooling Rate, Eq.(B3)

X	A_0	A_1	A_2	A_3	A_4	A_5	$x_1(X)^*$	$x_2(X)^*$
C	1970.	4570.	4160.	1870.	417.	37.0	0.0	0.09
N	-197.	-243.	-74.5	31.3	21.7	3.30	0.8	0.18
O	652.	1840.	1980.	1060.	280.	29.3	0.2	0.73

* x_1 are the cation mixing ratios for the Contemporary Earth and x_2 are the cation mixing ratios for the Early Earth.

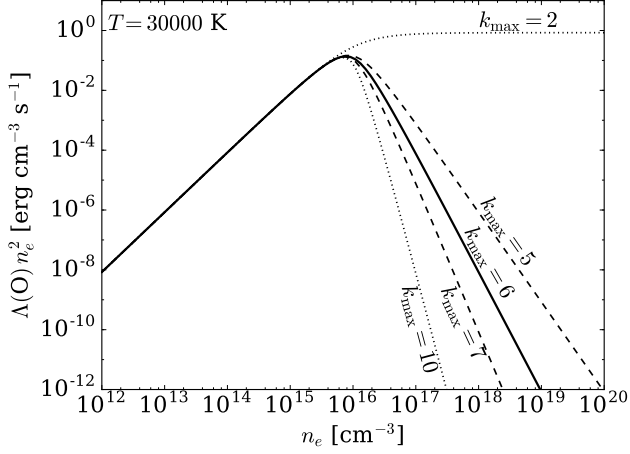


Figure B1. The total cooling rate, Λn_e^2 [erg cm⁻³ s⁻¹] for Oxygen, as a function of electron density n_e [cm⁻³], from Eq. (B4), with different values of k_{\max} ranging from 2 to 10 with $k_{\max} = 6$, the value used in the rest of this paper, represented with a solid line. Without these corrections, the cooling rate will increase when $n_e > 10^{16}$ cm⁻³ at the same slope as when $n_e < 10^{16}$ cm⁻³.

rates for the range of investigated densities overlap with the proposed cooling rate (see, e.g. Voitke et al. 1996). Because of the physical density dependency of our cooling rate and the reasonable agreement between our cooling rate and chemical and physical observation of lightning on Earth, we have good reason to think that we are representing the cooling from a lightning shock with sufficient accuracy for our work.

This paper has been typeset from a $\text{T}_{\text{E}}\text{X}/\text{L}^{\text{A}}\text{T}_{\text{E}}\text{X}$ file prepared by the author.